Rotobreather dynamics in underdamped Josephson junction ladders

1999 J. Phys.: Condens. Matter 11 321

(http://iopscience.iop.org/0953-8984/11/1/027)

J. Phys.: Condens. Matter **11** (1999) 321–334. Printed in the UK PII: S0953-8984(99)96553-0

Rotobreather dynamics in underdamped Josephson junction ladders

S Flach†§ and M Spicci‡‖

† Max-Planck-Institut für Physik komplexer Systeme, Nöthnitzer Strasse 38, D-01187 Dresden, Germany

‡ Nonlinear Centre, DAMTP, Silver Street, Cambridge CB3 9EW, UK

Received 5 August 1998, in final form 30 September 1998

Abstract. We study rotobreather properties in Josephson ladders with external dc currents and nonzero island–island capacitances. These solutions are localized in space, with tails characterized by exponential localization and a wave length which both vary smoothly upon varying the external bias. We demonstrate the existence of resonances for underdamped systems which are related to the plane wave spectrum of the nonresistive system. We propose experimental observations of these resonances.

1. Introduction

It is a well established fact that classical Hamiltonian lattices which generate nonlinear equations of motion for the participating degrees of freedom generically allow for time-periodic spatially localized solutions, coined discrete breathers ([A], [FW] and references therein). Remarkably these excitations exist in the absence of any disorder. The main reason for their existence and structural stability is the boundness of the associated eigenvalue problem for small amplitudes where the equations of motion can be linearized around some homogeneous and translationally invariant minimum of the total energy. Originally these discrete breathers corresponded to localized oscillations on such a lattice. Considerations of Hamiltonian systems with periodicity in the 'displacements' (e.g. coupled pendula) lead to the observation that rotobreather solutions also exist, i.e. solutions where certain pendula perform rotational motion, while pendula far away from the breather centre librate with amplitudes decaying with increasing distance [TP1], [TP2], [MA]. Extensions of these concepts to more general evolution equations of coupled degrees of freedom showed that localization takes place also in nonHamiltonian systems [MS]. Consequently it became of considerable interest to consider certain geometries of small coupled Josephson junctions, as these systems under proper circumstances can be described using classical equations of motion for the superconducting phase differences of the junctions. A recently proposed ladder geometry [FM] could serve as an ideal candidate to perform experimental studies in order to observe rotobreather states. Indeed, Josephson junction systems have been extensively used in the past as a playground for various nonlinear excitations on the one hand (e.g. [UCM]), while this knowledge has been applied to the studies of properties of cuprates and related materials on the other hand [KM], [HKUM].

§ E-mail address: flach@mpipks-dresden.mpg.de.

‖ E-mail address: m.spicci@damtp.cam.ac.uk.

0953-8984/99/010321+14$19.50

Rotobreather solutions in models of Josephson junction ladders have been considered in [FM]. There, the external current was assumed to be purely of ac type. The breather solutions phase lock, in these cases, to the external time-periodic driving. One consequence of this is that the amplitudes of oscillation will not decay to zero far from the breather centre. On the other hand, the frequencies of the assumed ac current should be of the order of the characteristic plasma frequencies (in order to ensure the validity of the used equations). This is not easy to realize experimentally. Indeed, experiments are usually carried out using dc currents. In that case, however, trivial phase locking no longer takes place. The frequencies of excited states will be some functions of the strength of the dc current. Although this seems to complicate the story, it does provide a nice possibility to continuously tune excited state properties by varying the dc current strength. Another reason to consider rotobreathers here is the fact that in experimental realizations the capacitive interaction between two superconducting islands is usually much stronger than the capacitive interaction between a given island and the substrate. In terms of the system energy [WS]

$$H = \frac{1}{2}\sum C_{ij}V_iV_j - \frac{1}{2}E_{ij}\cos(\theta_i - \theta_j)$$

(here V_i is the voltage on the ith island), this implies that offdiagonal terms of the capacitance matrix C_{ij} will be large compared to the diagonal ones. The equations considered in [WS] assume diagonal capacitance matrices. A comparison to experiments should take offdiagonal terms into account.

Recently MacKay and Sepulchre [MS] proved the existence of rotobreather solutions in a simplified model with dc currents. This result can be grasped in the following way: a single Josephson junction shows coexistence of a stable limit cycle (rotating state, nonzero voltage drop) and a stable fixed point (time-independent phase difference, no voltage drop) for external currents below the critical value, provided the junction is underdamped. A set of uncoupled junctions can then be prepared in such a way that one junction is in the limit cycle while all others are in the fixed point (with same external currents applied at each junction). Switching on some weak coupling between the junctions (in practice the couplings will be junctions again) keeps the localization property of the state provided the coupling is short ranged.

The aim of this paper is to consider the equations of the Josephson ladder and to study rotobreather properties and their dependence on the external dc current. The paper is organized in the following way. In section 2 we consider the model and the plane wave spectrum (when neglecting resistive terms). In section 3 we show how to generate rotobreathers experimentally, and discuss numerically obtained solutions. Section 4 is devoted to the tail analysis of rotobreathers, and the effects of varying the external current strength. We conclude with consequences for experiments.

2. The model

We consider a 2D array of small Josephson junctions arranged in a ladder geometry (see figure 1), i.e. two rows of junctions in series connected by a parallel array of other junctions, with $N_j = 2N + 1$ loops (or cells). The inductive effects due to the weak links and the finite size of the electrodes, are also explicitly taken into account by means of inductances in series with each junction. Hereafter φ_n^H (respectively $\tilde{\varphi}_n^H$) will denote the gauge-invariant phase-difference (PD) between the order parameters of the right and left superconducting electrodes at the interface of the nth lower (respectively upper) horizontal junction, and φ_n^V the corresponding PD between the upper and lower superconductors of the vertical junction lying on the left side of the same cell. In addition, we assume that the array is fed by independent

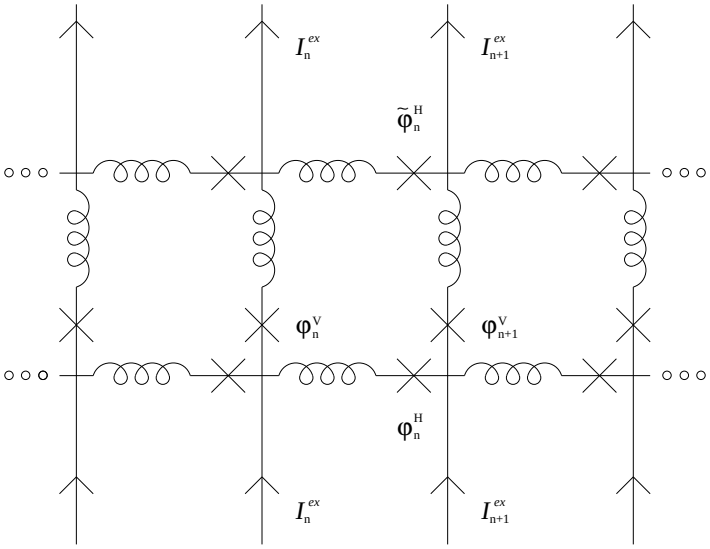

Figure 1. The equivalent electrical network of the model. The '×' represent Josephson junctions.

current generators which inject currents at each node of the lower row, and extract them at the corresponding one of the upper row.

The equations of motion governing the time evolution of the PD in this model are derived in [GF], where the following assumptions are made: (1) the mutual inductance between any pair of cells is negligible with respect to the self-inductance of each of them; (2) all cells are identical; (3) the dependence of the junction critical currents on the magnetic flux through the junction interface is negligible; (4) the current flowing in each junction is described by the resistive-shunted-junction (RSJ) model [BP], [T]. Unlike [GF], in our approach the vertical and horizontal junctions may have in general different values of the capacitance, resistance and critical current (anisotropic ladder), provided these parameters satisfy the following relations

$$r \doteq \frac{C^V}{I_c^V} = \frac{C^H}{I_c^H} \tag{1}$$

$$p \doteq I_c^V R^V = I_c^H R^H. \tag{2}$$

Notice also that the assumption made in [GF], that the currents injected (and extracted) are all equal, can be replaced by the more general condition that the current injected in a node of the lower row and that extracted from the corresponding one in the upper row are equal. Therefore, we may use the indexed quantity I_n^{ex} to denote the current flowing through the generator connected to the nth pair of nodes of the ladder. In addition, by virtue of this symmetry between upper and lower nodes, the PD of the two horizontal junctions of a cell obey the same equation, up to the sign of the current flowing through them. This implies that if we choose initial conditions which have the above symmetry, the time evolution of $\tilde{\varphi}_n^H$ and φ_n^H will be the same (up to a sign), so that we may write $\tilde{\varphi}_n^H \equiv -\varphi_n^H$. Since we will always assume that this is the case, we may limit our consideration to the dynamics of φ_n^V and φ_n^H, whose equations of motion read [GF]

$$\ddot{\varphi}_n^V + \alpha\dot{\varphi}_n^V + \sin\varphi_n^V = \gamma_n + \beta_L(2(\varphi_n^H - \varphi_{n-1}^H) + \varphi_{n+1}^V + \varphi_{n-1}^V - 2\varphi_n^V) \tag{3}$$

$$\ddot{\varphi}_n^H + \alpha\dot{\varphi}_n^H + \sin\varphi_n^H = \frac{\beta_L}{\eta}(\varphi_n^V - \varphi_{n+1}^V - 2\varphi_n^H) \tag{4}$$

where

- time is measured in units of $\tau \doteq \sqrt{(\Phi_\circ/2\pi)r}$ ($\Phi_\circ = h/e$ is the flux quantum);
- the dissipation coefficient is $\alpha = 1/\sqrt{\beta_C}$, where $\beta_C \doteq 2\pi r p^2/\Phi_\circ$ [McC];
- $\gamma_n \doteq I_n^{ex}/I_c^V$;
- $\beta_L \doteq \Phi_\circ/(2\pi L I_c^V)$, where L is the self-inductance of a cell [McC];
- $\eta \doteq I_c^H/I_c^V$ is the anisotropy parameter;
- $n = 0, \pm 1, \pm 2, \ldots, \pm N$.

In the following we will assume periodic boundary conditions

$$\varphi^V_{n+N_j} \equiv \varphi^V_n \tag{5}$$

$$\varphi^H_{n+N_j} \equiv \varphi^H_n . \tag{6}$$

The plane wave dispersion relation associated to this model in the absence of dissipation ($\alpha = 0$), is calculated by linearizing equations (3) and (4), introducing $\hat{\varphi}^V_n \doteq \varphi^V_n - \gamma_n$ and assuming the following ansatz for the solutions

$$\hat{\varphi}^V_n \propto \sum_q \xi_q \, \mathrm{e}^{\mathrm{i}(qn-\omega(q)t)} \tag{7}$$

$$\varphi^H_n \propto \sum_q \theta_q \, \mathrm{e}^{\mathrm{i}(qn-\omega(q)t)} \tag{8}$$

where q is the wave vector. By inserting these relations into equations (3) and (4), and requiring that the determinant of the resulting set of algebraic equations vanishes, in order to have nontrivial solutions for the Fourier amplitudes ξ_q and θ_q, we finally obtain a linear dispersion relation consisting of two branches, namely

$$\omega^{(1)}_p = 1 \tag{9}$$

$$\omega^{(2)}_p(q) = \sqrt{1 + \frac{2\beta_L}{\eta} + 4\beta_L \sin^2\frac{q}{2}}. \tag{10}$$

Notice that the lower branch, $\omega^{(1)}_p$, is dispersionless†. The Fourier amplitude patterns corresponding to $\omega^{(1)}_p$ and $\omega^{(2)}_p$ verify

$$\xi_q \neq 0 \qquad \theta_q = 0 \qquad q = 0$$

$$\frac{\xi_q}{\theta_q} = \frac{2}{1-\mathrm{e}^{\mathrm{i}q}} \qquad q \neq 0$$

and, respectively,

$$\xi_q = 0 \qquad \theta_q \neq 0 \qquad q = 0$$

$$\frac{\xi_q}{\theta_q} = -\eta(1-\mathrm{e}^{-\mathrm{i}q}) \qquad q \neq 0.$$

3. Excitation of rotobreathers

The procedure through which a rotobreather can be excited in an underdamped Josephson junction ladder, consists of three steps.

† This symmetry is a result of Kirchhoff's laws together with the chosen geometry of the system. Other geometries might lift this symmetry, leading to a nonzero dispersion in the lower branch. Since this dispersion will still be bounded due to the spatial discreteness of the system, the existence and properties of rotobreathers will be not qualitatively changed [FW].

(1) Initially, just one current generator is turned on, e.g., the one connected to the 0th pair of nodes, and we let it inject a current $\gamma_0 = \gamma^{(1)} > 1$. Therefore, as the stationary state has been reached, a localized excitation of the PD is established along the ladder, with φ_0^V rotating (φ_{-1}^H and φ_0^H do the same, see below) and all the others performing forced oscillations around the minimum of the potential with the same frequency.

(2) After reaching the stationary state in the first phase, the current is decreased to a new value $\gamma^{(2)} < 1$, such that a localized excitation may be still sustained by the array.

(3) Finally, after relaxing the system into the steady state, all the remaining current generators are switched on, giving rise to a uniform pattern of bias currents $\gamma_n = \gamma^{(2)} < 1$, $n = 0, \pm 1, \pm 2, \ldots, \pm N$.

We will now show some numerical results which illustrate the above procedure. Starting from the initial conditions $\varphi_n^V(0) = \varphi_n^H(0) = 0$ and $\dot{\varphi}_n^V(0) = \dot{\varphi}_n^H(0) = 0$ for $n = 0, \pm 1, \pm 2, \ldots, \pm N$, we have numerically integrated the equations of motion of a ladder with $N_j = 11$ cells, by using a fifth-order Cash–Karp Runge–Kutta algorithm, combined with an embedded fourth-order method for the estimate of the truncation error. We have considered the following values for the parameters: $\alpha = 0.1$, $\beta_L = 1.0$ and $\eta = 1.0$. In addition, the first two phases described above have been chosen of lengths $T^{(1)} = T^{(2)} = 500$ (natural units) with $\gamma^{(1)} = 2$ and $\gamma^{(2)} = 0.7$.

The pairs of figures, 2 and 3, 4 and 5, and 6 and 7 below, show the time evolution of the PD velocities of some vertical and horizontal junctions on the left of the 0th pair of nodes, respectively at the end of the first phase, at the end of the second phase and, after a long time, during the third phase. Notice that the system, except for the horizontal junctions in the Nth cell, is symmetric around the 0th vertical junction, so that the same results are obtained on the rhs of the latter (up to the sign of $\dot{\varphi}_n^H$, $n = 0, 1, 2, \ldots, N-1$). In all these plots one can recognize the rotating motions of φ_0^V and φ_{-1}^H by the nonzero average of the corresponding velocities. By comparing such averages one concludes that the following relations hold

$$\langle \dot{\varphi}_{-1}^H \rangle = -\langle \dot{\tilde{\varphi}}_{-1}^H \rangle = -\frac{\langle \dot{\varphi}_0^V \rangle}{2} \tag{11}$$

and similarly

$$\langle \dot{\varphi}_0^H \rangle = -\langle \dot{\tilde{\varphi}}_0^H \rangle = \frac{\langle \dot{\varphi}_0^V \rangle}{2}. \tag{12}$$

These can be explained by recalling that the time average of the PD velocity is proportional to the voltage drop across the junction barrier and that the sum of the voltages around a cell must vanish. By using equations (11) and (12) one may also obtain a general approximate relation between $\langle \dot{\varphi}_0^V \rangle$, γ_0, α and η. Let us consider the equations of motion of the central vertical and horizontal junctions

$$\ddot{\varphi}_0^V + \alpha \dot{\varphi}_0^V + \sin \varphi_0^V = \gamma_0 + \beta_L (2(\varphi_0^H - \varphi_{-1}^H) + \varphi_1^V + \varphi_{-1}^V - 2\varphi_0^V) \tag{13}$$

$$\ddot{\varphi}_0^H + \alpha \dot{\varphi}_0^H + \sin \varphi_0^H = \frac{\beta_L}{\eta} (\varphi_0^V - \varphi_1^V - 2\varphi_0^H) \tag{14}$$

$$\ddot{\varphi}_{-1}^H + \alpha \dot{\varphi}_{-1}^H + \sin \varphi_{-1}^H = \frac{\beta_L}{\eta} (\varphi_{-1}^V - \varphi_0^V - 2\varphi_{-1}^H). \tag{15}$$

Upon combining them together, one easily obtains

$$\ddot{\varphi}_0^V + \alpha \dot{\varphi}_0^V + \sin \varphi_0^V = \gamma_0 + \eta (\ddot{\varphi}_{-1}^H - \ddot{\varphi}_0^H + \alpha (\dot{\varphi}_{-1}^H - \dot{\varphi}_0^H) + \sin \varphi_{-1}^H - \sin \varphi_0^H)$$

If we now take the time average of this expression, use equations (11) and (12) and neglect the contributions of the sines, we find

$$\langle \dot{\varphi}_0^V \rangle \approx \frac{\gamma_0}{\alpha(1+\eta)} \tag{16}$$

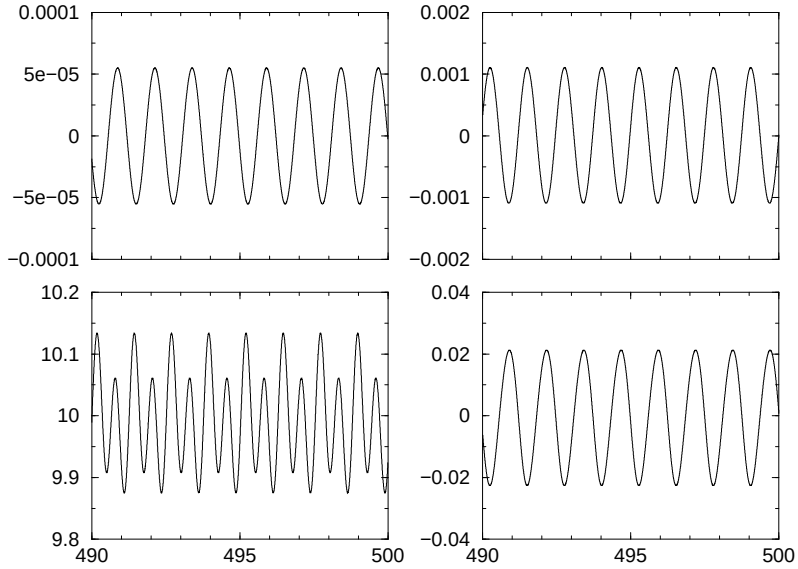

Figure 2. Dynamics of the vertical junctions in local injection regime with $\gamma_0 = 2$. Clockwise from the left-hand upper square: $\dot{\varphi}^V_{-3}$, $\dot{\varphi}^V_{-2}$, $\dot{\varphi}^V_{-1}$ and $\dot{\varphi}^V_0$ as functions of time (natural units) for $\alpha = 0.1$, $\beta_L = 1.0$ and $\eta = 1.0$. Ladder with $N_j = 11$ cells.

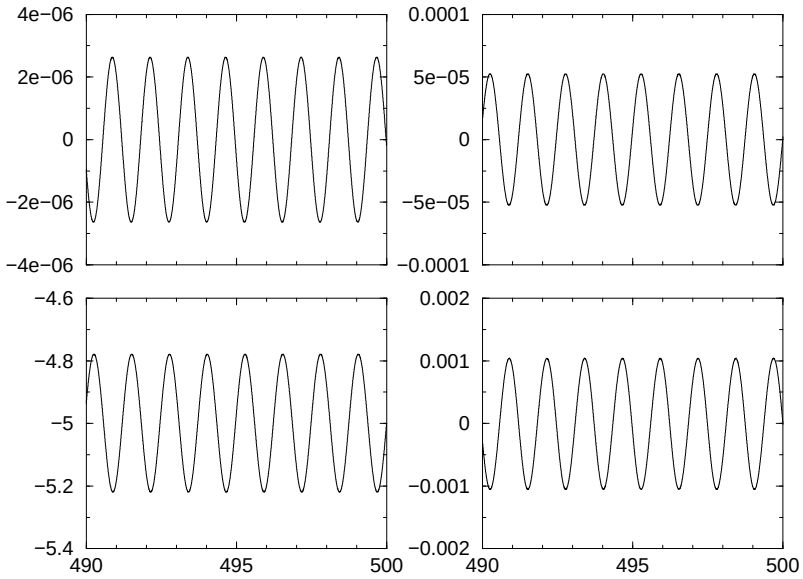

Figure 3. Dynamics of the horizontal junctions in local injection regime with $\gamma_0 = 2$. Clockwise from the left-hand upper square: $\dot{\varphi}^H_{-4}$, $\dot{\varphi}^H_{-3}$, $\dot{\varphi}^H_{-2}$ and $\dot{\varphi}^H_{-1}$ as functions of time (natural units) for $\alpha = 0.1$, $\beta_L = 1.0$ and $\eta = 1.0$. Ladder with $N_j = 11$ cells.

since in the steady state the averages of the accelerations vanish. Upon taking a look at figures 2 and 3, it is seen that this simple relation is fairly well satisfied during the first phase.

Another interesting aspect of our results is noteworthy. The excitation obtained for $\gamma_0 = 2.0$ (see figures 2 and 3) appear to be more strongly localized about the 0th vertical

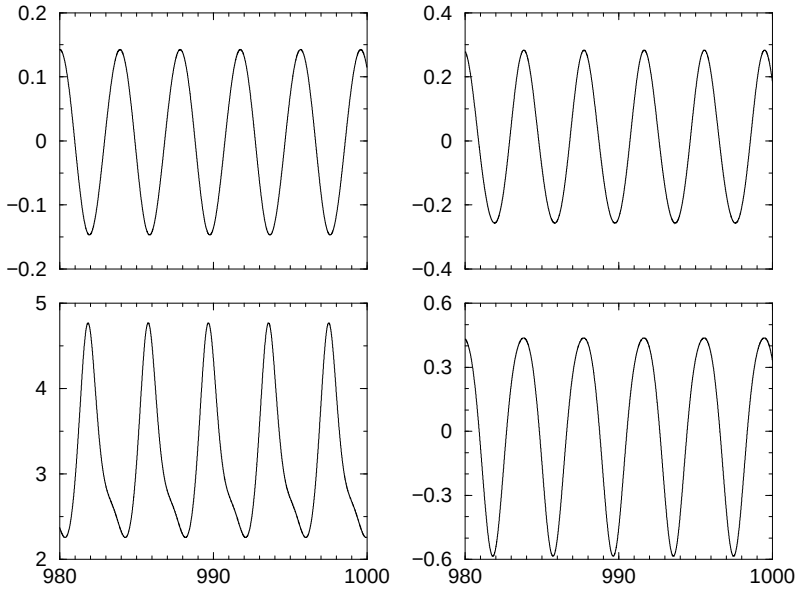

Figure 4. Dynamics of the vertical junctions in local injection regime with $\gamma_0 = 0.7$. Clockwise from the left-hand upper square: $\dot{\varphi}^V_{-3}$, $\dot{\varphi}^V_{-2}$, $\dot{\varphi}^V_{-1}$ and $\dot{\varphi}^V_0$ as functions of time (natural units) for $\alpha = 0.1$, $\beta_L = 1.0$ and $\eta = 1.0$. Ladder with $N_j = 11$ cells.

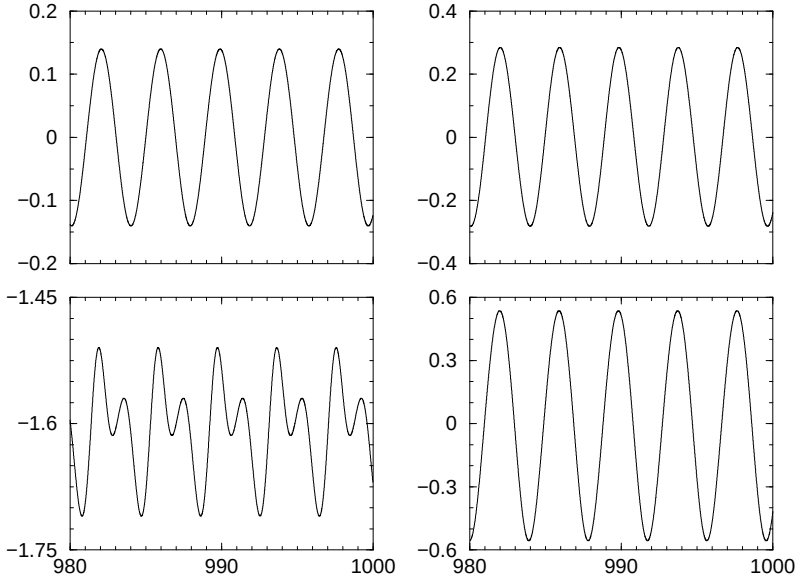

Figure 5. Dynamics of the horizontal junctions in local injection regime with $\gamma_0 = 0.7$. Clockwise from the left-hand upper square: $\dot{\varphi}^H_{-4}$, $\dot{\varphi}^H_{-3}$, $\dot{\varphi}^H_{-2}$ and $\dot{\varphi}^H_{-1}$ as functions of time (natural units) for $\alpha = 0.1$, $\beta_L = 1.0$ and $\eta = 1.0$. Ladder with $N_j = 11$ cells.

junction than that observed after decreasing the driving current to $\gamma_0 = 0.7$ (see figures 4 and 5). In addition, for $\gamma_0 = 2.0$ the PD of two adjacent junctions of the same class (vertical or horizontal) oscillate approximately with opposite phases, whereas for $\gamma_0 = 0.7$ they vibrate

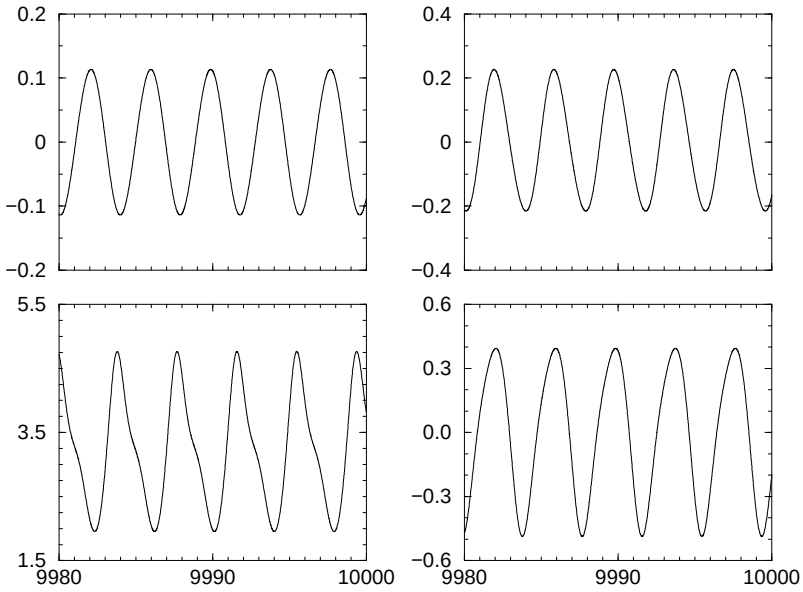

Figure 6. Rotobreather dynamics of the vertical junctions. Clockwise from the left-hand upper square: $\dot{\varphi}^V_{-3}$, $\dot{\varphi}^V_{-2}$, $\dot{\varphi}^V_{-1}$ and $\dot{\varphi}^V_0$ as functions of time (natural units) for $\alpha = 0.1$, $\beta_L = 1.0$ and $\eta = 1.0$. Ladder with $N_j = 11$ cells uniformly fed with $\gamma_n = 0.7$, $n = 0, \pm 1, \ldots, \pm N$.

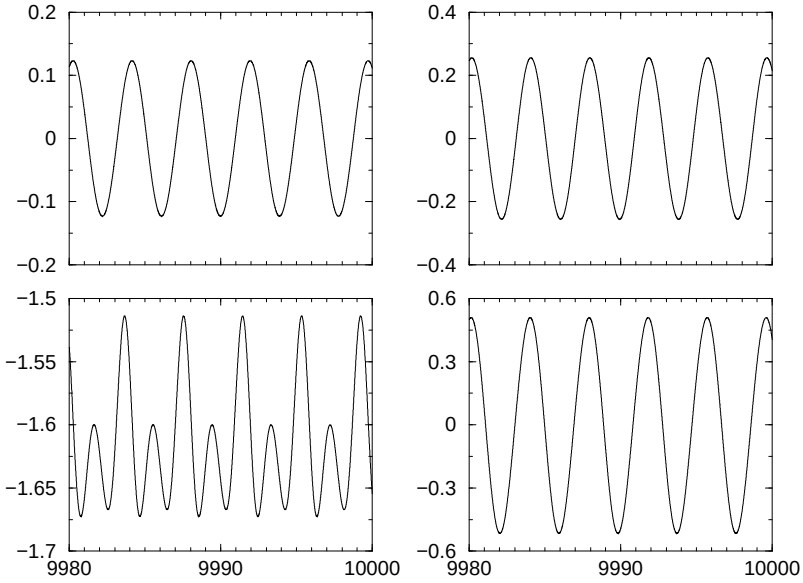

Figure 7. Rotobreather dynamics of the horizontal junctions. Clockwise from the left-hand upper square: $\dot{\varphi}^H_{-4}$, $\dot{\varphi}^H_{-3}$, $\dot{\varphi}^H_{-2}$ and $\dot{\varphi}^H_{-1}$ as functions of time (natural units) for $\alpha = 0.1$, $\beta_L = 1.0$ and $\eta = 1.0$. Ladder with $N_j = 11$ cells uniformly fed with $\gamma_n = 0.7$, $n = 0, \pm 1, \ldots, \pm N$.

approximately in phase. The origin of these effects is that a rotobreather is characterized by a localization rate and phase shifts that depend on the driving current through the frequency of oscillation ω of the vibrating PD (notice that $\omega \approx 5.0$ for $\gamma_0 = 2.0$ and $\omega \approx 1.6$ for

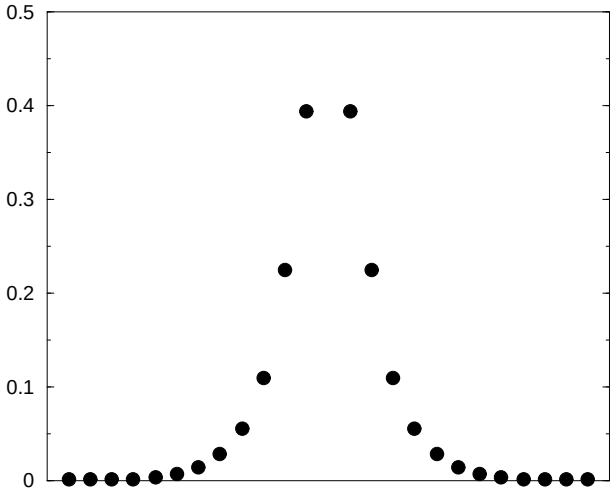

Figure 8. Rotobreather profile: amplitudes of the oscillating vertical PD velocities for a ladder with $N_j = 25$. The other parameters are as before.

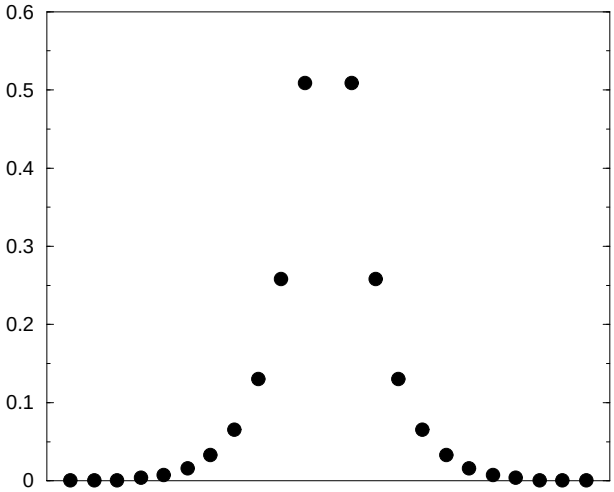

Figure 9. Rotobreather profile: amplitudes of the oscillating horizontal PD velocities for a ladder with $N_j = 25$. The other parameters are as before.

$\gamma_0 = 0.7$). This point will be clarified in the next section, where we derive analytically both the localization rate and the phase shifts of our rotobreathers, starting from the ansatz of time periodicity for the solution of equations (3) and (4).

Finally, figures 8 and 9 show the amplitudes of oscillation of the PD velocities associated to the vertical and, respectively, horizontal junctions which lie on the left and on the right of the central rotating junctions, in a ladder with $N_j = 25$ and the same parameters as in figures 6 and 7. As is seen, the amplitudes decay to zero for both types of junctions, showing that the rotobreather solution of our system is spatially decaying into static fixed points. This is in contrast to [FM], where the amplitudes, due to the periodic driving, were not decaying to zero far away from the rotobreather centre.

4. Analysis of the tails of a rotobreather

In both local and uniform current injection regimes, the presence of a single rotobreather in the ladder is characterized far from its centre, i.e. along the tails, by vertical and horizontal junctions whose PD perform vanishing oscillations around the minimum of the potential. This allows us to develop a general analysis of several properties of the rotobreather, particularly localization rate and phase shifts, by considering the linearized equations of motion of the system. It is to be mentioned that a similar approach has been used recently in [UMS], where the dynamics of bunched fluxon states in a discrete Josephson transmission line were considered. In that case the analysis of the tails of the kinks travelling along the line, permitted the evaluation (approximately) of the kink velocities at which the switching between different bunched states takes place.

The details of our analysis are as follows. By linearizing equations (3) and (4), one finds

$$\ddot{\varphi}_n^V + \alpha\dot{\varphi}_n^V + \varphi_n^V = \Gamma_n + \beta_L(2(\varphi_n^H - \varphi_{n-1}^H) + \varphi_{n+1}^V + \varphi_{n-1}^V - 2\varphi_n^V) \tag{17}$$

$$\ddot{\varphi}_n^H + \alpha\dot{\varphi}_n^H + \varphi_n^H = \frac{\beta_L}{\eta}(\varphi_n^V - \varphi_{n+1}^V - 2\varphi_n^H) \tag{18}$$

where

$$\Gamma_n = \begin{cases} 0 & \text{local injection regime} \\ \gamma & \text{uniform injection regime} \end{cases}$$

and $|n| \gg 1$. If we now define $\hat{\varphi}_n^V \doteq \varphi_n^V - \Gamma_n$, equations (17) and (18) become

$$\ddot{\hat{\varphi}}_n^V + \alpha\dot{\hat{\varphi}}_n^V + \hat{\varphi}_n^V = \beta_L(2(\varphi_n^H - \varphi_{n-1}^H) + \hat{\varphi}_{n+1}^V + \hat{\varphi}_{n-1}^V - 2\hat{\varphi}_n^V) \tag{19}$$

$$\ddot{\varphi}_n^H + \alpha\dot{\varphi}_n^H + \varphi_n^H = \frac{\beta_L}{\eta}(\hat{\varphi}_n^V - \hat{\varphi}_{n+1}^V - 2\varphi_n^H). \tag{20}$$

Let us search for the periodic solutions to (19) and (20), for some fixed period $T = 2\pi/\omega$. The periodicity of the solution allows us to expand the components $\hat{\varphi}_n^V$ and φ_n^H in Fourier series

$$\hat{\varphi}_n^V = \sum_\kappa \hat{\Phi}_\kappa^V \, \mathrm{e}^{\Lambda(\kappa)n + \mathrm{i}\kappa\omega t} \tag{21}$$

$$\varphi_n^H = \sum_\kappa \Phi_\kappa^H \, \mathrm{e}^{\Lambda(\kappa)n + \mathrm{i}\kappa\omega t} \tag{22}$$

with

$$\Lambda(\kappa) = \mathcal{R}(\kappa) + \mathrm{i}\,\mathcal{I}(\kappa) \tag{23}$$

and $\kappa = 0, \pm 1, \pm 2, \ldots$. By inserting (21) and (22) in (19) and (20) and equating coefficients corresponding to the same κ, one obtains the following algebraic equations in the Fourier amplitudes $\hat{\Phi}_\kappa^V$ and Φ_κ^H

$$\left(\kappa^2\omega^2 + \mathrm{i}\,\alpha\kappa\omega - 1 + 4\sinh^2\frac{\Lambda}{2}\right)\hat{\Phi}_\kappa^V + 2\beta_L(1 - \mathrm{e}^{-\Lambda})\Phi_\kappa^H = 0 \tag{24}$$

$$\frac{\beta_L}{\eta}(1 - \mathrm{e}^{\Lambda})\hat{\Phi}_\kappa^V + \left(\kappa^2\omega^2 + \mathrm{i}\alpha\kappa\omega - 1 - 2\frac{\beta_L}{\eta}\right)\Phi_\kappa^H = 0. \tag{25}$$

In order to have nontrivial solutions, the determinant of the latter set of equations must vanish. That leads to a complex algebraic equation in Λ, which can be split in a pair of real equations into the unknowns

$$x \doteq \mathrm{Re}\left(\sinh^2\frac{\Lambda}{2}\right) \tag{26}$$

$$y \doteq \mathrm{Im}\left(\sinh^2\frac{\Lambda}{2}\right) \tag{27}$$

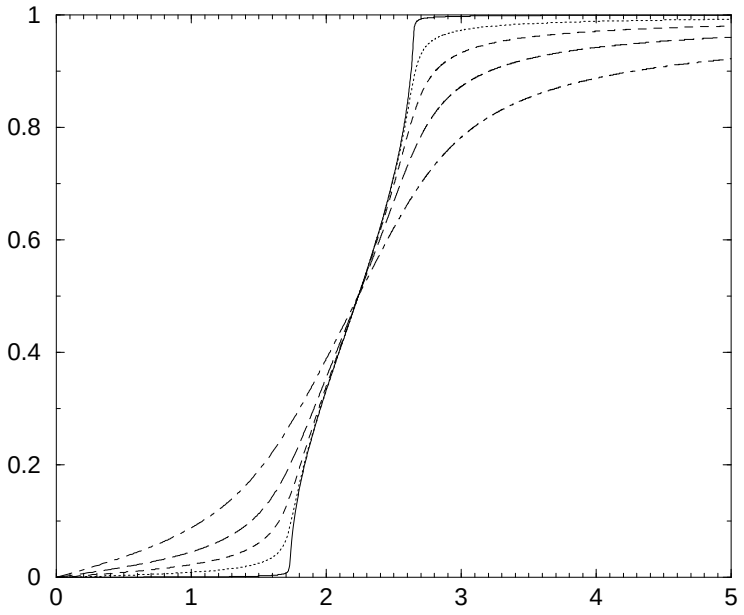

Figure 10. $\mathcal{I}/\pi$ as a function of $|\kappa\omega|$ for $\beta_L = 1.0$, $\eta = 1.0$ and $\alpha = 0.01$ (solid), 0.1 (dotted), 0.25 (dashed), 0.5 (long-dashed), 1.0 (dot-dashed).

namely

$$4\beta_L(\kappa^2\omega^2 - 1)x + 4\beta_L\alpha\kappa\omega y + \kappa^4\omega^4 - \left(2 + \alpha^2 + \frac{2\beta_L}{\eta}\right)\kappa^2\omega^2 + 1 + \frac{2\beta_L}{\eta} = 0$$

$$4\beta_L\alpha\kappa\omega x - 4\beta_L(\kappa^2\omega^2 - 1)y - 2\alpha\kappa^3\omega^3 - 2\alpha\kappa\omega\left(1 + \frac{\beta_L}{\eta}\right) = 0.$$

As one can easily check, for $\alpha = 0$ and $|\kappa\omega| = 1$ the set cannot determine any solution for x and y, since all coefficients vanish. This corresponds to the linear plane wave mode $\omega_p^{(1)}$ (see (9)), which is dispersionless. On the other hand, for $\alpha \neq 0$ the above set has a unique solution for any value of $\kappa\omega$, i.e.

$$x = \frac{1 + 2\beta_L/\eta - \kappa^2\omega^2}{4\beta_L} \tag{28}$$

$$y = \frac{\alpha\kappa\omega}{4\beta_L}. \tag{29}$$

We now wish to invert (28) and (29) and make the dependence of $\mathcal{R}$ and $\mathcal{I}$ on $|\kappa\omega|$ explicit. We first notice (see appendix for details) that equations (26) and (27) can be manipulated to get the form

$$\cosh^2\mathcal{R}\cos^2\mathcal{I} \quad = (1 + 2x)^2 \tag{30}$$

$$\cosh^2\mathcal{R} + \cos^2\mathcal{I} = 1 + 4y^2 + (1 + 2x)^2. \tag{31}$$

Then, if we introduce the equation

$$\xi^2 - (1 + 4y^2 + (1 + 2x)^2)\xi + (1 + 2x)^2 = 0 \tag{32}$$

we find the following solution for $\mathcal{R}$ and $\mathcal{I}$

$$\mathcal{R} = \operatorname{arcosh}(\sqrt{\xi_+}) \leqslant 0 \tag{33}$$

$$\mathcal{I}_\pm = \arccos(\pm\sqrt{\xi_-}) \tag{34}$$

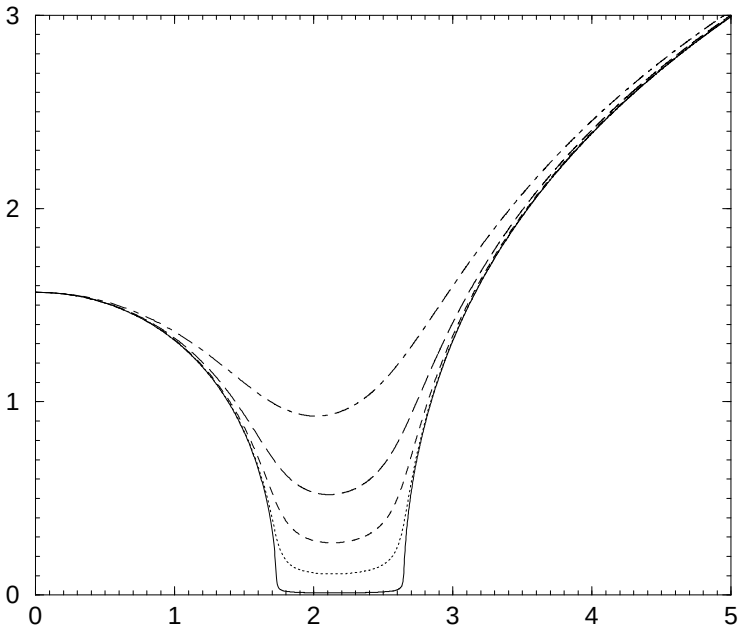

Figure 11. $|\mathcal{R}|$ as a function of $|\kappa\omega|$ for $\beta_L = 1.0$, $\eta = 1.0$ and $\alpha = 0.01$ (solid), 0.1 (dotted), 0.25 (dashed), 0.5 (long-dashed), 1.0 (dot-dashed).

where

$$\xi_\pm = \tfrac{1}{2}(1 + 4y^2 + (1 + 2x)^2 \pm \sqrt{16y^4 + (1 - (1 + 2x)^2)^2 + 8y^2(1 - (1 + 2x)^2)^2})$$

(it is easy to see that $\xi_+ \geqslant 1$ and $\xi_- \leqslant 1$ for any x and y).

With the help of the above derived relations it is easy to compute all tail properties. Let us focus here on one aspect. When considering breathers in Hamiltonian lattices, the imaginary part of Λ is fixed by the wave number of a plane wave with a frequency belonging to the edge of the band, and e.g. in systems with nearest neighbour interaction this will be either $q = 0$ or $q = \pi$, independently of ω. Here however we find that $\mathcal{I}$ becomes a smooth function of ω, which is due to the dissipative terms in the equations of motion. Thus a given rotobreather will be characterized not only by a given localization length, but also by a characteristic wave length in the tails. In figures 10 and 11 we show the dependences of $\mathcal{I}$ and $\mathcal{R}$ on $\kappa\omega$ for different values of α. The transition to the Hamiltonian case is nicely observed in figure 10. The strong variation of $\mathcal{I}$ is observed when $\kappa\omega$ is tuned through the position of the plane wave spectrum (which is defined for $\alpha = 0$). Remarkably the localization length $1/\mathcal{R}$ is also not diverging for nonzero α anymore when $\kappa\omega$ belongs to the plane wave spectrum, in contrast to the Hamiltonian case $\alpha = 0$. Thus breathers become even more robust in nonHamiltonian systems, although the resonances which are deadly in the Hamiltonian case can be still traced in the dissipative case.

5. Conclusions

In this paper we presented a study of rotobreather solutions in Josephson ladders with injected dc currents and nonzero island–island capacitances. By that we expect to be close

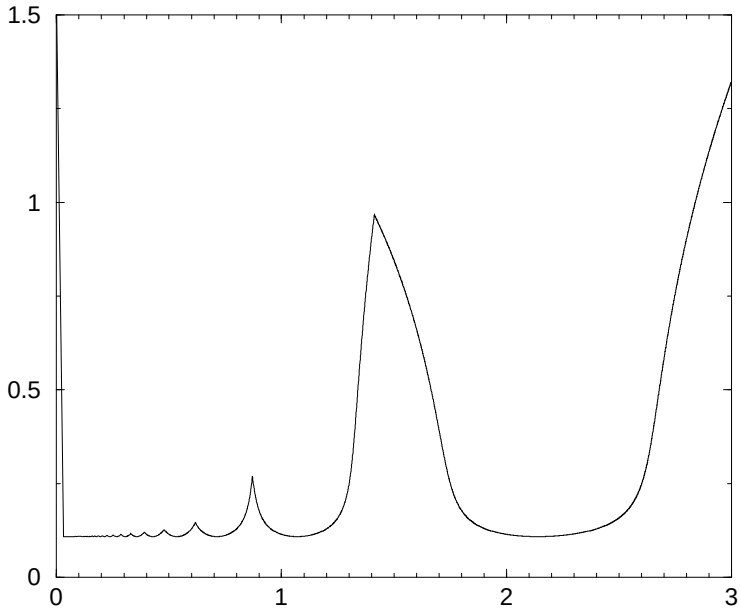

Figure 12. Minimal curve $|\mathcal{R}_{min}|$ as a function of $|\omega|$ calculated for $\kappa = 1, \ldots, 100$. Parameters: $\beta_L = 1.0$, $\eta = 1.0$ and $\alpha = 0.1$.

to experimental realizations of these systems. We showed that rotobreathers do exist, and that the tails of these solutions are characterized both by a localization length and by a wave length which change simultaneously upon changing the frequency of the solution. We proposed a simple way to generate these solutions experimentally. Let us finally propose some experimental observations. If one succeeds in generating a rotobreather experimentally, one could change the bias. By that one will smoothly change the rotobreather frequency, and consequently also all its multiples $\kappa\omega$. The first prediction is then that in the tails of the solution one should observe not only a smooth change of the localization length, but also a smooth change of the wavelength. Both effects could be detected. Furthermore, whenever a multiple $\kappa\omega$ crosses the plane wave spectrum, resonances are expected, i.e. the localization length should increase (but not diverge) and the wave length should vary much more strongly (see figures 10 and 11). If one succeeds in varying the current such that several resonances are covered, the inverse localization length $\mathcal{R}$ should vary as depicted in figure 12, which is generated by taking the minimum of $\mathcal{R}(\kappa)$ for any given ω. These resonance patterns will be clear fingerprints of the presence of rotobreathers in Josephson ladders. Experiments are on the way to confirm these predictions.

Acknowledgment

We wish to thank A V Ustinov for stimulating discussions.

Appendix

By virtue of equation (23), we have

$$\sinh\frac{\Lambda}{2} = \sinh\frac{\mathcal{R}}{2}\cos\frac{\mathcal{I}}{2} + \mathrm{i}\cosh\frac{\mathcal{R}}{2}\sin\frac{\mathcal{I}}{2} \tag{35}$$

which gives

$$\sinh^2\frac{\Lambda}{2}=\sinh^2\frac{\mathcal{R}}{2}\cos^2\frac{\mathcal{I}}{2}-\cosh^2\frac{\mathcal{R}}{2}\sin^2\frac{\mathcal{I}}{2}+2\mathrm{i}\,\sinh\frac{\mathcal{R}}{2}\cosh\frac{\mathcal{R}}{2}\sin\frac{\mathcal{I}}{2}\cos\frac{\mathcal{I}}{2}. \tag{36}$$

Therefore, by means of the following identities

$$\sin\mathcal{I}=2\sin\frac{\mathcal{I}}{2}\cos\frac{\mathcal{I}}{2} \tag{37}$$

$$\sinh\mathcal{R}=2\sinh\frac{\mathcal{R}}{2}\cosh\frac{\mathcal{R}}{2} \tag{38}$$

$$\sin^2\frac{\mathcal{I}}{2}=\frac{1-\cos\mathcal{I}}{2} \tag{39}$$

$$\cos^2\frac{\mathcal{I}}{2}=\frac{\cos\mathcal{I}+1}{2} \tag{40}$$

$$\sinh^2\frac{\mathcal{R}}{2}=\frac{\cosh\mathcal{R}-1}{2} \tag{41}$$

$$\cosh^2\frac{\mathcal{R}}{2}=\frac{\cosh\mathcal{R}+1}{2} \tag{42}$$

one can write equations (26) and (27) in the form

$$x=\frac{\cosh\mathcal{R}\cos\mathcal{I}-1}{2} \tag{43}$$

$$y=\frac{\sinh\mathcal{R}\sin\mathcal{I}}{2} \tag{44}$$

By squaring these latter and using the basic relations $\sin^2\mathcal{I}+\cos^2\mathcal{I}=1$, $\cosh^2\mathcal{R}-\sinh^2\mathcal{R}=1$ we finally obtain equations (30) and (31).

References

[A] Aubry S 1997 Breathers in nonlinear lattices: existence, linear stability and quantization *Physica* D **103** 201

[BP] Barone A and Paternò G 1982 *Physics and Application of the Josephson Effect* (New York: Wiley)

[FW] Flach S and Willis C R 1998 Discrete breathers *Phys. Rep.* **295** 181

[FM] Floría L M, Marín J L, Martínez P J, Falo F and Aubry S 1996 Intrinsic localisation in the dynamics of a Josephson-junction ladder *Europhys. Lett.* **36** 539

[GF] Grimaldi G, Filatrella G, Pace S and Gambardella U 1996 Flux distribution and critical currents in a one-dimensional row of a Josephson junction square lattice *Phys. Lett.* A **223** 463

[HKUM] Hechtfischer G, Kleiner R, Ustinov A V and Müller P 1997 Non-Josephson emission from intrinsic junctions in $Bi_2Sr_2CaCu_2O_{8+y}$: Cherenkov radiation by Josephson vortices *Phys. Rev. Lett.* **79** 1365

[KM] Kleiner R and Müller P 1994 Intrinsic Josephson effects in high-T_c superconductors *Phys. Rev.* B **49** 1327

[MS] MacKay R S and Sepulchre J A 1998 Stability of discrete breathers *Physica* D **119** 148

[MA] Marin J L and Aubry S 1996 Breathers in nonlinear lattices: numerical calculation from the anticontinuous limit *Nonlinearity* **9** 1501

[McC] McCumber D E 1968 Effect of ac impedance on dc voltage-current characteristic of superconductor weak-link junctions *J. Appl. Phys.* **39** 3113

[TP1] Takeno S and Peyrard M 1997 Nonlinear rotating modes: Green's function solution *Phys. Rev.* E **55** 1922

[TP2] Takeno S and Peyrard M 1996 Nonlinear modes in coupled rotator models *Physica* D **92** 140

[T] Tinkham M 1996 *Introduction to Superconductivity* 2nd edn (New York: McGraw-Hill)

[UCM] Ustinov A V, Cirillo M and Malomed B A 1993 Fluxon dynamics in one-dimensional Josephson-junction arrays *Phys. Rev.* B **47** 8357

[UMS] Ustinov A V, Malomed B A and Sakai S 1998 Bunched fluxon states in one-dimensional Josephson-junction arrays *Phys. Rev.* B **57** 11 691

[WS] Wang ZQ and Stroud D 1991 Dynamics of granular superconductors at zero and large magnetic fields: glassy behaviour *Phys. Rev.* B **44** 9743